Hindawi
Complexity
Volume 2020, Article ID 5641596, 10 pages
https://doi.org/10.1155/2020/5641596

Research Article

Cyber-Enabled Intelligence Control and Security Optimization for Complex Microgrid Networks Transient Frequency Stability Analysis of Power Systems considering Photovoltaic Grid Connection

Jun Wu,[1] Xiangyu Xing,[1] Chen Wu,[2] Baolin Li,[1] Wei Huang,[2] Peiying Gan,[1] and Hui Zhou[1]

[1]*School of Electrical Engineering & Automation, Wuhan University, Wuhan 430072, China*
[2]*Yunnan Power Grid Co., Ltd., Kunming 650000, China*

Correspondence should be addressed to Xiangyu Xing; 2015302540146@whu.edu.cn

Received 26 May 2020; Revised 28 August 2020; Accepted 16 September 2020; Published 12 October 2020

Academic Editor: Jingang Lai

Copyright © 2020 Jun Wu et al. This is an open access article distributed under the Creative Commons Attribution License, which permits unrestricted use, distribution, and reproduction in any medium, provided the original work is properly cited.

In view of the photovoltaic grid-connected power system, the transient frequency stability of the system is analyzed in this paper. First, the photovoltaic grid-connected power system was modeled and analyzed. On this basis, the maximum frequency deviation is used as the index to determine the interval in which the system accommodates the maximum photovoltaic capacity, and the influence of frequency stability of the high-permeability photovoltaic high disturbance system is studied. Second, the evaluation and prediction methods of frequency dynamic characteristics of photovoltaic access nodes based on surface fitting are proposed, and the critical values of high penetration photovoltaic access for different grid points are given. Finally, an improvement measure based on the optimization of the frequency modulation parameters of large-capacity units is proposed, and the effectiveness of the proposed method in improving the transient frequency stability of the system after photovoltaic access is verified by the IEEE 39-standard system.

1. Introduction

Solar photovoltaic technology, as a universal and endless clean energy power generation method with the largest utilization potential, has attracted the attention of power practitioners and researchers. However, photovoltaic output is characterized by randomness, intermittence, no mechanical rotational inertia, and no participation in system frequency modulation, which brings new challenges to power grid control, making it difficult for the existing control mode to ensure the safety of power system. Therefore, at the level of mechanism analysis, there is necessity of (a) in-depth study of the mechanism of photovoltaic access on the frequency stability of power systems and (b) simulation verification based on the model of photovoltaic power generation units, with theoretical guidance on how to improve the system's transient stability after grid connection. Stability evaluation involves (a) study of the frequency characteristics of system nodes after photovoltaic grid connection and (b) proposing the evaluation method of system frequency support capability, which has reference value to engineering practice. Stability improvement measures are concerned with feasible measures for frequency modulation after photovoltaic grid connection, which has practical significance for the safe and stable operation of power systems.

A lot of relevant research has been carried out at home and abroad. With the promotion of microgrid technology, research on its control [1, 2] and other aspects is aimed at achieving flexible and efficient applications of distributed energy in various forms and huge quantities. Jingang Lai and his colleagues [3] proposed a cluster-oriented cooperative control strategy for multiple AC microgrids clusters, which enables maximum utilization of distributed energy resources.

In addition, a distributed cooperative control scheme is also proposed in order to implement a distributed secondary control for hybrid lossy microgrids, and sufficient conditions on the requirements for the network connectivity and the delays boundedness are presented, which guarantees the stability and synchronization of the controlled hybrid lossy microgrid power systems [4].

Connecting distributed photovoltaic to the distribution network in the form of microgrids is an effective way to solve grid frequency stability and other issues after photovoltaic grid connection. For the research on the transient model of photovoltaic power generation systems, the studies in [5–7] modeled modules such as photovoltaic arrays, power electronic converters, and their control systems, reviewed the research status of the entire photovoltaic power generation system model, and then summarized the method of using the above basic component model to build an overall model of a photovoltaic power generation system. Zhang et al. [8] adopted the Simulink simulation software to construct a MATLAB experimental simulation model of the photovoltaic power generation system, using the classic control algorithm-maximum power point tracking control and a subunit of relay protection logic control. Wang et al. [9] adopted the method of indirect combination modeling, in which the device-level electromechanical transient model was first established in the PSD-BPA environment, including the electromechanical transient model of typical doubly fed fans, energy storage units, and the photovoltaic power generation unit. Based on the device-level modeling, a power plant-level model was established, and the equivalent method was specifically used to realize the combination of the electromechanical transient models of the three combined power generation systems. Then, the correctness of the model was constructed and verified by numerical simulation under BPA environment.

In addition to focusing on the modeling of photovoltaic grid-connected systems to improve their performance, domestic and foreign scholars have also carried out studies on the frequency stability of photovoltaic grid-connected systems [10–15]. Kakimoto et al. and Zhou et al. [16, 17] believed that the key factor affecting the frequency stability of the system was the primary frequency regulation of the unit, so that the stability of the power system was likely to be significantly improved by setting reasonable adjustment coefficients and governor parameters. Du [18] studied the high-frequency problems caused by the system splitting after the new energy grid connection and analyzed the different impacts of the different settings of the protection definite value for the over-speed protection control of thermal power units. Du also studied the low-frequency problem and proposed an optimization strategy for low-frequency load shedding to solve the problem of increasing frequency of low-frequency load shedding. For Chen et al. [19], in order to improve the frequency stability of the grid-connected photovoltaic system, the control strategy of the optical storage grid-connected inverter based on virtual synchronous generators was studied, and the inertia and damping were introduced into the power control link to simulate a synchronous generator to achieve a frequency modulation and voltage regulation. Zheng et al. [20] studied the dynamic frequency characteristics of the power system under the impact of unbalanced power in the scenario of high-permeability photovoltaic and proposed countermeasures to improve the frequency characteristics from three aspects: changing inertia constant, changing mechanical power regulation performance, and changing generator electromagnetic power.

Based on the above analysis, this paper proposes a method to achieve system transient frequency stability caused by photovoltaic grid connection. Firstly, based on the modeling of photovoltaic grid-connected networks, the influence of large grid disturbances on frequency stability under the condition of high photovoltaic penetration is analyzed, and the maximum frequency deviation is used as an indicator to determine the maximum photovoltaic capacity of the system. Secondly, a method for evaluation and prediction of the frequency dynamic characteristics of photovoltaic access nodes based on surface fitting is proposed, and the critical values of high-permeability photovoltaic access at different grid-connected points can be calculated through the above method. Then, improvement measures based on optimization of frequency modulation parameters of large-capacity units are proposed to improve the transient frequency stability of the system after photovoltaic access. Finally, the validity of the proposed method is verified with an IEEE 39-node example.

2. Modeling of Photovoltaic Grid-Connected Systems

The power system simulation software PSD-BPA is used to build a transient model of each link of the photovoltaic grid-connected system in this paper. The photovoltaic power generation unit consists of three parts, namely, photovoltaic cell arrays, low-voltage box-type transformers, and voltage-type inverters. The topology of photovoltaic power generation unit is shown in Figure 1.

The photovoltaic grid-connected system model is composed of multiple photovoltaic power generation units and grid-connected system models. After the photovoltaic power generation units are connected in parallel, they are first boosted by a step-up transformer, and then the photovoltaic power generation system transmits the active power to the collection station via the 110 kV collection line. The photovoltaic grid-connected system includes parallel transmission of several photovoltaic power generation collection branches, and its topology is shown in Figure 2.

3. System Frequency Stability Impact of Large Disturbances in Photovoltaic High-Permeability Grids

3.1. Analysis of Mechanism. Based on the analysis of the frequency response characteristics of conventional units, this section studies the effect mechanism of the frequency stability of large disturbances in photovoltaic high-permeability grids. When the power system is disturbed, the electromagnetic power variation of the generator is affected

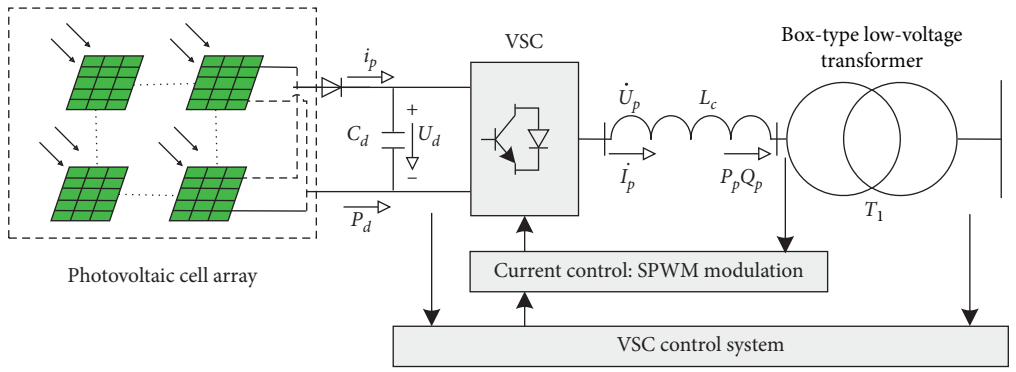

Figure 1: Topology of photovoltaic power generation unit.

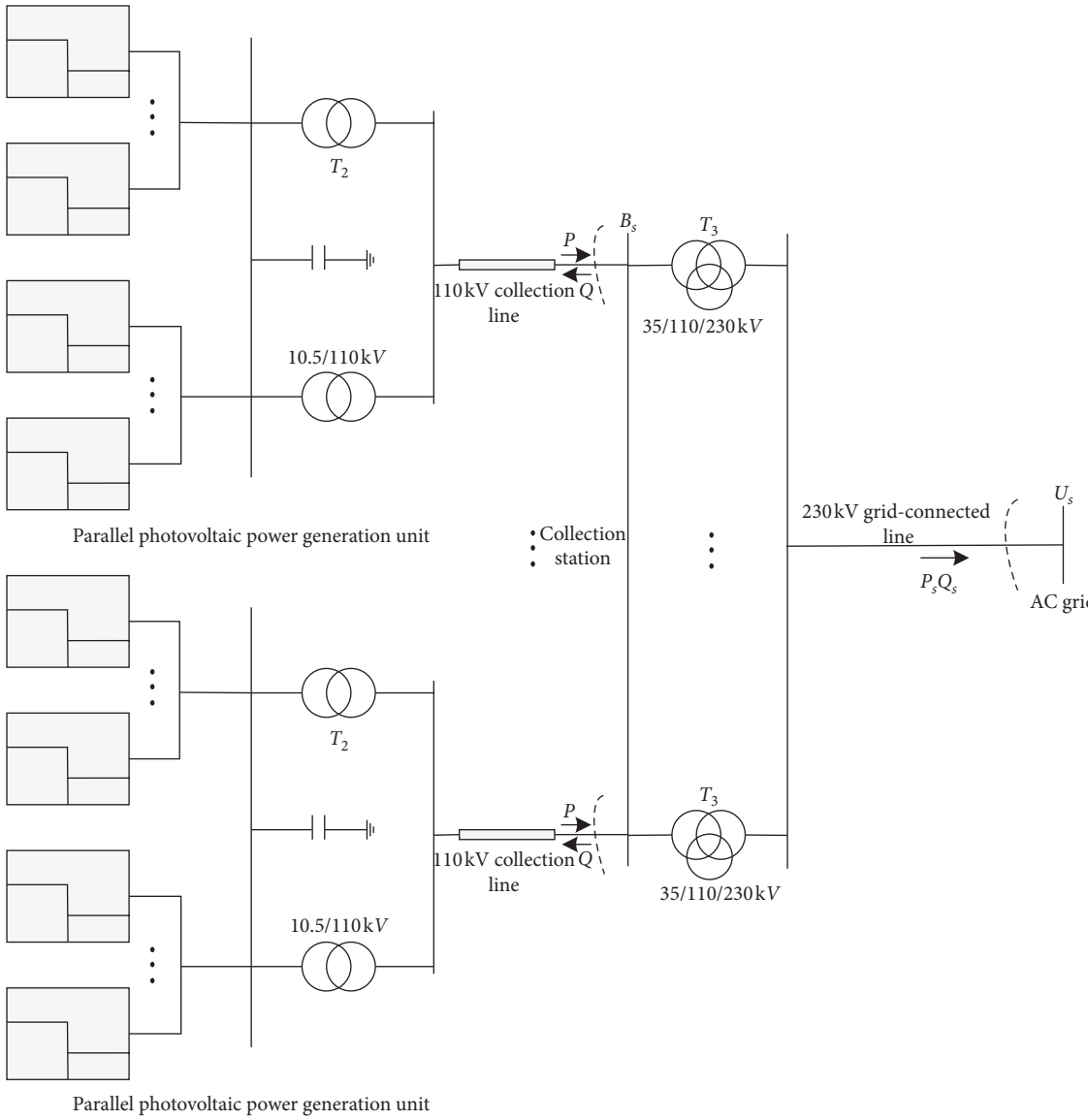

Figure 2: Photovoltaic grid-connected system model.

by factors such as power grid conditions and the primary frequency modulation of the unit, and the variation is complicated. In order to simplify the analysis, the method of using the inertia coefficient to calculate the constant distribution ratio is used in this paper to describe the change of the electromagnetic power.

When a system with n conventional generator sets has a multiple fault at node k, equation (1) is obtained, wherein ΔP_{ei} and ΔP represent the change of the electromagnetic power and disturbance power of the ith generator set; P_{sik} is the full-step power coefficient between nodes i and k; T_{ji} and R_i represent the inertia time constant and adjustment coefficient of the ith generator:

$$\begin{cases} \Delta P_{ei}(0^+) = -\left(\dfrac{P_{sik}}{\sum_{i=1}^{n} P_{sik}}\right)\Delta P, \\ \Delta P_{ei}(t) = -\left(\dfrac{T_{Ji}}{\sum_{i=1}^{n} T_{Ji}}\right)\Delta P, \\ \Delta P_{ei}(\infty) = -\dfrac{1}{R_i}\dfrac{\Delta P}{\sum_{i=1}^{n}(1/R_i)}. \end{cases} \tag{1}$$

After photovoltaic is connected to the power grid, m of the n conventional units in the system are replaced with photovoltaic generators. As m increases continuously, the system's moment of inertia decreases. At this time, the full-step coefficients, moments of inertia, and reactive power compensation coefficients of all conventional units are assumed to be identical. If the disturbance of multiple fault occurs in the photovoltaic grid-connected system, equation (2) is obtained:

$$\begin{cases} \Delta P_{ei}(0^+) = \left(\dfrac{P_{sik}}{\sum_{i=1}^{n'} P_{sik}}\right)\Delta P = \dfrac{1}{n'}\Delta P, \\ \Delta P_{ei}(t) = \dfrac{T_{Ji}\Delta P}{\sum_{a=1}^{m} T_{Ja} + \sum_{i=1}^{n'} T_{Ji}} = \dfrac{1}{n'}\Delta P, \\ \Delta P_{ei}(\infty) = -\dfrac{1}{R_i}\dfrac{\Delta P}{\sum_{a=1}^{m} 1/R_a + \sum_{i=1}^{n'} 1/R_i} = -\dfrac{1}{n'}\Delta P. \end{cases} \tag{2}$$

In equation (2), n is the number of remaining conventional units.

From equation (2), it can be seen that, under large disturbances, as the photovoltaic permeability of the system increases, the remaining conventional units bear more power shortage, and the instantaneous changes in electromagnetic power and steady-state deviations are more obvious; that is, the problem of transient frequency stability in the system is easier to detect.

3.2. Effect of Photovoltaic Output with Different Permeability on System Frequency Fluctuation. Based on IEEE 39-node standard calculation examples, this section uses PSD-BPA software simulation to verify and analyze the impact of photovoltaic power generation systems on the dynamic frequency characteristics of the system caused by factors such as output characteristics when large disturbances occur at different permeability. Figure 3 shows the geographical wiring diagram of the IEEE 39-node standard calculation system. The parameters are as follows: the reference capacity is 100 MW, the reference voltage is 100 kV, and the total generator installed capacity is 5,620 MW, of which the generator at node 31 is a balancing machine.

As the installed capacity of conventional units at bus 39 is the largest, which is 1000 MW, we may integrate the photovoltaic power station into the power grid through bus 2, and set the photovoltaic permeability at 0~100% of the installed capacity of conventional units at bus 39. With the help of PSD-BPA software simulation, the frequency dynamic characteristics of the system when large disturbances occur at different permeabilities are obtained, including the minimum and highest frequency dynamic processes of the system and the dynamic processes of the node frequency of the public access point bus 1 and the node bus 39, which is the largest load and is close to the grid connection point. Among them, the two major disturbance faults sets are as follows:

(1) Three-phase short circuit fault occurred on the branch bus 6–bus 11 at the fifth cycle and was cleared at the tenth cycle

(2) When increasing the photovoltaic active power output, the active power output of a conventional unit is cut off in the same proportion

The simulation results are shown in Figures 4 and 5, where Figure 4 is the dynamic curve of the minimum and highest frequency of the system, Figure 5(a) shows the dynamic curve of the frequency of node 1, and Figure 5(b) shows the dynamic curve of the frequency of node 39.

From Figures 4 and 5, it is known that the minimum and maximum frequency of the system and the dynamic frequency of bus 1 and bus 39 nodes change with the different photovoltaic permeability. Figure 4 indicates that the minimum and maximum dynamic frequency of the system have the same change trend, and under the disturbance condition, the photovoltaic high-permeability system may exceed the upper or the lower limit of the frequency; that is, there will be high- and low-frequency problems. Therefore, when evaluating the frequency stability of the system, the absolute value of the frequency deviation should be used as a reference index. The main reason is that as the photovoltaic permeability increases, the system inertia decreases, the remaining conventional units bear more power shortage, and the instantaneous changes in electromagnetic power and steady-state deviations are more obvious, so that the power angle is more likely to destabilize.

For example, in Figure 5, the difference of frequency dynamic between the permeability of 50% and 100% may be caused by factors such as voltage instability. With the increase of photovoltaic penetration, the dynamic frequency change process of the system is shown in Table 1 (unit: Hz).

Since the maximum frequency fluctuation allowed by the grid under the condition of a small system capacity is ±0.5 Hz, it is clear from Table 1 that the maximum acceptable photovoltaic penetration rate of this system is 20%~

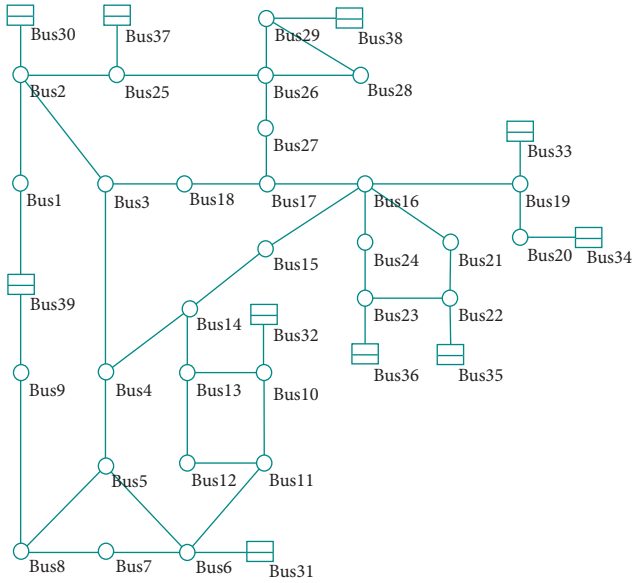

Figure 3: IEEE 39-node standard example geographic wiring diagram.

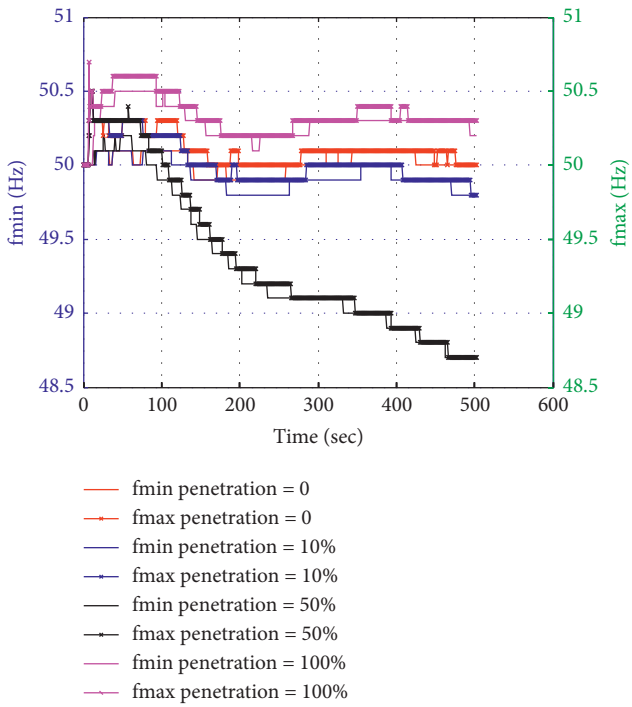

Figure 4: Minimum and maximum frequency dynamics of the system when different permeability fails.

30%; that is, the maximum installed capacity of photovoltaic falls in the range of 200 MW~ 00 MW. However, the critical photovoltaic installed capacity is difficult to give by the method of ergodic simulation test adopted in this section. The above analysis shows that the photovoltaic grid-connected frequency prediction and evaluation method proposed has great application reference value for determining the photovoltaic grid-connected points and its installed capacity in engineering practice. In fact, as long as any two of the three indicators are given in the method proposed in this article, the remaining one can be determined. Therefore, it is completely feasible to use this method to analyze the frequency characteristics after photovoltaic grid connection.

4. Evaluation Analysis and Prediction Method of the Frequency Dynamic Characteristics of Photovoltaic Access Nodes

4.1. Method and Data Acquisition of Node Frequency Dynamic Characteristics. When the system is subject to a power disturbance ΔP, the power system frequency changes. The dynamic frequency characteristic of a system is the time process when the system transitions from a normal state to another stable value. In this paper, the absolute value of the maximum node frequency deviation of all node frequencies in this dynamic process is used as a frequency index to characterize this process, as shown in

$$\Delta f = \left|\Delta f_{\max}\right| = \max\left(\left|f_{\max} - f_N\right|, \left|f_{\min} - f_N\right|\right). \quad (3)$$

At the same time, the electrical distance is used as an important index to measure the spatiotemporal distribution characteristics when the disturbance occurs at different locations. The length of the electrical distance is generally described by the size of the transfer reactance between the two points. When a large disturbance produces an active power shortage, the instantaneous unbalanced power at the initial stage of the disturbance is distributed among the units through an inverse proportional to the electrical distance.

This section is based on the IEEE 39 node standard calculation example. With the help of the PSD-BPA simulation software, a series of experimental data of $(\Delta P, S, \Delta f)$ were obtained by the ergodic simulation to change the position of the disturbance point and the amount of disturbance in the power flow file and the steady-state file multiple times.

4.2. Surface Generation and Analysis Method of Node Frequency Characteristic Based on Surface Fitting. Adopting the methods in the previous sections, we perform cubic spline interpolation on the obtained experimental data. By writing MATLAB program, the surface fitting of "frequency deviation-electrical distance-photovoltaic permeability" was realized. That is, the surface fitting of node frequency characteristics is studied based on the given discrete data.

In order to accurately calculate the frequency deviation value under different disturbances and electrical distances, interpolation and fitting methods were used for accurate data processing, and the modified B-spline method was used to correct the nonsmooth surface fitted by the finite data points obtained from BPA simulation. Generally, the more control points to fit the surface are followed by higher accuracy, but the calculation is more complicated, and there is also more occurrence of singular phenomenon. Therefore, the number of initial control points should be minimized to satisfy accuracy.

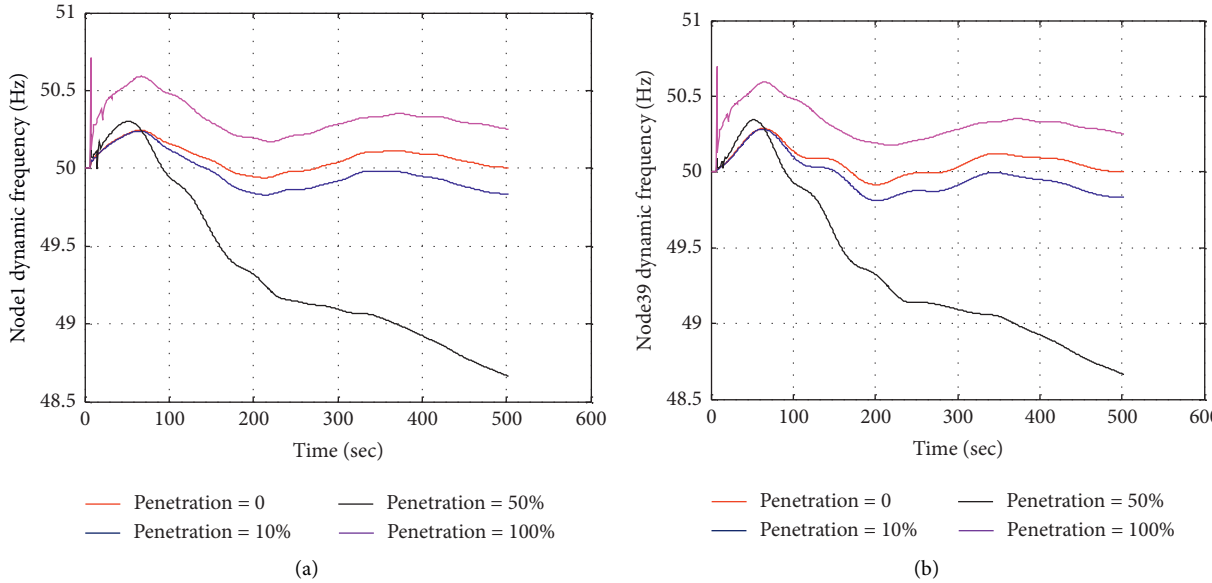

Figure 5: Frequency dynamics of node 1 and node 39 when different permeability fails.

Table 1: Frequency dynamic response of the system when different PV permeability fails.

Photovoltaic penetration (%)	Minimum bus frequency (Hz)	Maximum bus frequency (Hz)	Absolute maximum frequency deviation (Hz)
0	49.994602	50.011600	0.011600
10	49.830513	49.844547	0.169487
20	49.657547	49.669304	0.342453
30	49.441223	49.452263	0.558777
40	49.141018	49.149567	0.858982
50	48.660889	48.671333	1.339111

Finally, the accuracy of the fitted surface is verified according to

$$G = \frac{\Delta f - \Delta f'}{\Delta f'} \times 100\%. \quad (4)$$

In equation (4), Δf and $\Delta f'$ are the fitted and simulated values of the frequency index.

4.3. Analysis of Examples. In the IEEE 39-node system, the photovoltaic access node bus 2 is selected as the observation point, and the cutoff points are sequentially selected as bus 32, bus 35, bus 38 and bus 39, and the disturbance amount is sequentially set to 0.1, 0.2, 0.3, 0.4, 0.5, and 0.6. That is, the installed photovoltaic capacity is 100 MW, 200 MW, 300 MW, 400 MW, 500 MW, and 600 MW. The simulation was performed with the help of power system simulation software PSD-BPA, and 6 groups of experimental data were calculated according to equation (3).

By using the *B*-spline surface fitting method, the above experimental data were interpolated and then fitted to obtain the node frequency characteristic surface under disturbance, as shown in Figure 6.

The accuracy of the fitting results of the node frequency characteristics of the curved surface obtained by cubic interpolation of B-spline is calculated according to equation (4). The specific method is as follows: first, an electrical distance is determined to verify the accuracy of the absolute value of the frequency deviation under different disturbance amounts. Then, a disturbance quantity is determined in the same way to verify the accuracy of the absolute value of the frequency deviation under different disturbance amounts. Among them, the predicted value is read from the drawn surface according to the handle function in MATLAB. The specific accuracy verification results are shown in Table 2.

The accuracy verification shows that the node frequency and voltage characteristics prediction based on surface fitting proposed in this paper meets sufficient accuracy, and the error is less than 2%. Therefore, we can process the prediction results: let S take 0.0012, 0.0080, 0.0103, 0.0331, and other electrical distances, respectively, and use the MATLAB to handle function to take points on the drawn surface to get the corresponding ΔP, which is approximated as the critical value of photovoltaic permeability. For example, when S is 0.0012, the critical photovoltaic permeability corresponding to the frequency index is 272.4 MW, which has great application reference value in determining the photovoltaic

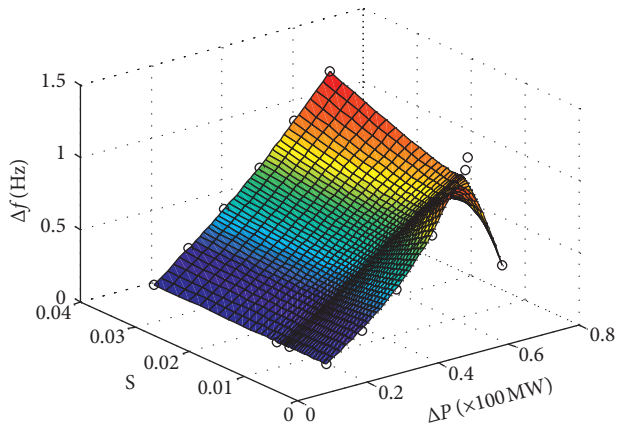

Figure 6: Node frequency characteristic surface under disturbance.

Table 2: Verification of the frequency index value when the disturbance amount and the electrical distance are, respectively, fixed.

ΔP	S	Δf	$\Delta f'$	G (%)
0.25	0.0148	0.408958	0.4158	1.6730
0.35	0.0148	0.591370	0.5946	0.5462
0.35	0.0295	0.59206	0.5964	0.7330

grid-connected point and its installed capacity in engineering practice.

5. Improvement Measures of Frequency Stability Based on Optimization of Frequency Regulation Parameters of Large-Capacity Units

5.1. Evaluation Index and Evaluation Method of Node Frequency Support Capability. In order to simplify the problem, in consideration of the transient frequency instability accident, the system frequency must first reach the trip conditions of triggering the generator set, and the transient frequency boundary condition of the unit trip is used as an index to evaluate the system frequency stability [21]. The definition of the frequency margin index of the node transient frequency offset safety is shown in

$$\eta = \frac{f'_{cr} - f_{cr}}{f_N - f_{cr}}. \tag{5}$$

In (5), f_N, f_{cr}, and f'_{cr} represent rated frequency value, generator high- and low-frequency protection value, and critical safety threshold, respectively. Node transient frequency offset safety is shown in Figure 7. Figure 7(a) reflects the relationship between the system frequency and time after the disturbance occurs. It can be seen that the system frequency finally stabilizes after a short and large fluctuation, and the frequency drops compared to before the disturbance. Figure 7(b) reflects the relationship between the system safety frequency margin index and the disturbance power. It can be seen from Figure 7(b) that when the disturbance reaches the critical value, the system frequency safety will be threatened.

Equation (5) shows that, in case of $\eta > 0$, the node transient frequency is safe; otherwise it is not safe; hence, $\eta = 0$ is critical safety. Similarly, the critical disturbance amount in Figure 7(b) can also be used as a determination condition whose value is calculated by interpolation according to

$$\Delta P_3 = \frac{\eta_2 \Delta P_1 - \eta_1 \Delta P_2}{\eta_2 - \eta_1}. \tag{6}$$

5.2. Analysis of Primary Frequency Regulation Parameters of Conventional Units. In this paper, the speed regulation system of a hydroturbine unit is taken as an example to analyze the influence of the optimization of one frequency regulation parameter on improving the frequency stability of the system. The model of the turbine governor and prime mover is shown in Figure 8.

Figure 8 indicates that the closed-loop transfer function of the governor is described as

$$\frac{P_M}{P_0 R - K' \Delta\omega} = \frac{(1/T_G(1 + sT_P))(1/s)(1 - sT_W/1 + s(T_W/2))}{1 + (R + (sD_d T_d/1 + sT_d))[(1/T_G(1 + sT_P))(1/s)]}. \tag{7}$$

According to the criterion of the generator dynamic stability characteristic equation, we can obtain

$$T_d{}^2 (R + D_d) + T_d (T_G + D_d T_P) + T_G T_P > 0. \tag{8}$$

In equation (8), the soft feedback coefficient is related to the water hammer effect time constant. Therefore, the main factors affecting the dynamic characteristics of the unit are the adjustment coefficient, the governor response time, and the time constant of the pilot valve.

The dead zone of the governor is also an important parameter that affects the system frequency. If set properly, the dead zone plays a role in filtering out disturbance signals with lower speeds and making the unit power stable. Conversely, if the dead zone set is too small, the unit is likely to be damaged because the valve is adjusted too frequently; if the dead zone set is too large, the frequency regulation ability is affected because the governor does not operate.

5.3. Effect of Frequency Modulation Parameter Optimization on Transient Frequency. Since the space for governor response time to be optimized is very limited, it is not feasible to operate the governor in actual engineering. Therefore, this article mainly studies the two aspects of optimizing the governing coefficient and the dead zone of the governor. Taking bus 32 as an example, the idea of simulation setup is as follows: (1) control the dead zone of the governor, set the adjustment coefficients to 0.02, 0.03, 0.04, 0.05, and 0.06, respectively, and calculate the critical disturbance of the system according to the above method; (2) the control adjustment coefficient remains unchanged, and the dead zone of the governor is set as 2r/min, 3r/min, 4r/min,

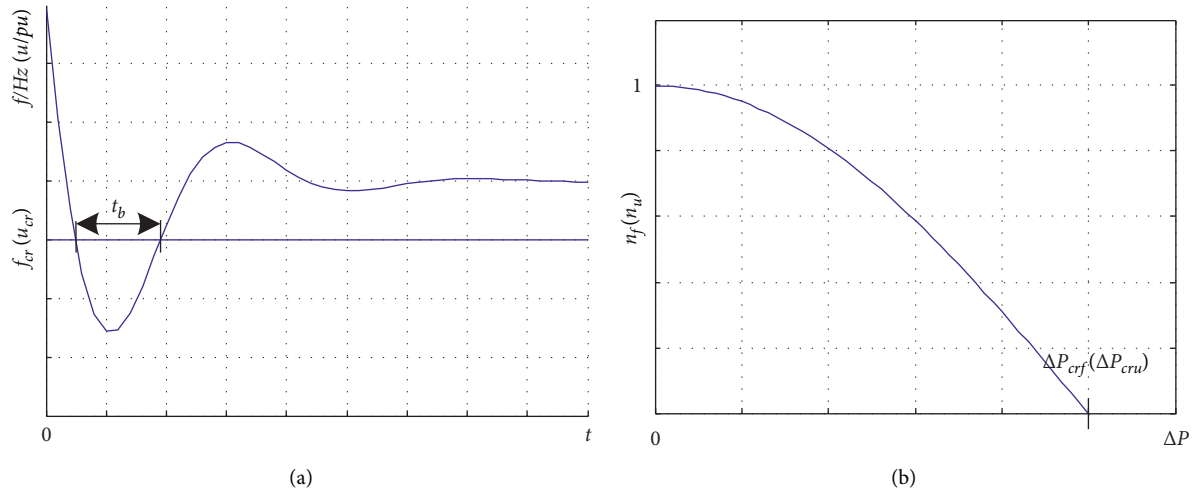

Figure 7: Node transient frequency offset security diagram.

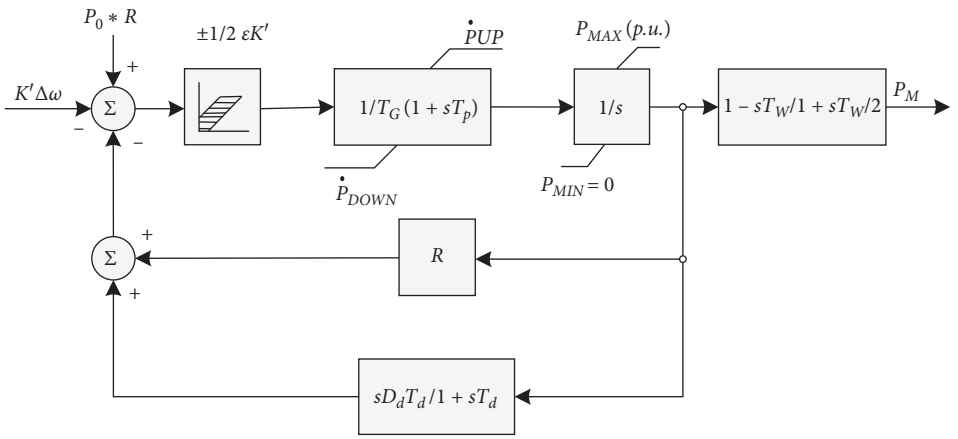

Figure 8: Typical structure of the turbine governor and prime mover model.

5r/min, and 6r/min. The critical disturbances of the system are calculated according to the above methods.

After simulation calculations, the results after optimized settings are shown in Figures 9 and 10.

From Figures 9 and 10, it can be seen that the critical disturbance amount that satisfies the frequency transient stability margin index seems to increase first and then decrease with the increase of the adjustment coefficient; as the dead zone of the governor increases, there is a tendency of monotonic decrease. Therefore, if the adjustment coefficient is too large or too small, the value of the frequency stability margin index decreases, and the corresponding critical disturbance amount also decreases accordingly. The size of the governor's dead zone determines the maximum frequency transient process and its maximum offset. The smaller governor dead zone set is followed by smaller maximum value of the frequency offset during the transient process, and the fluctuation process is smaller too.

Combining the above simulation experiments and analysis results, we can conclude that when the frequency stability margin index is considered to be satisfied in the

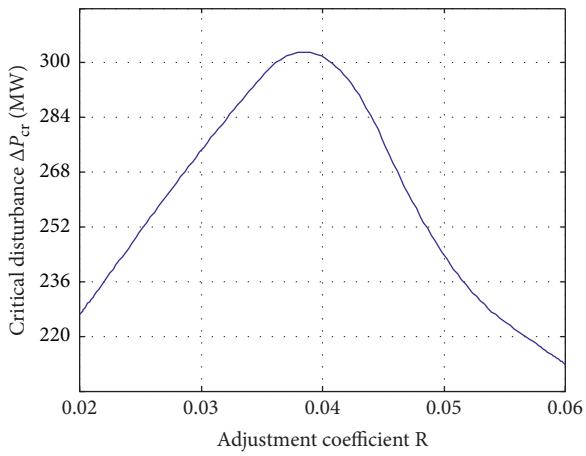

Figure 9: Critical disturbance amount curve after optimization of adjustment coefficient.

IEEE 39-node example, setting the frequency adjustment parameter of the large-capacity unit to the adjustment coefficient $R = 0.04$ and $\varepsilon = 2$r/min is optimal. At this time,

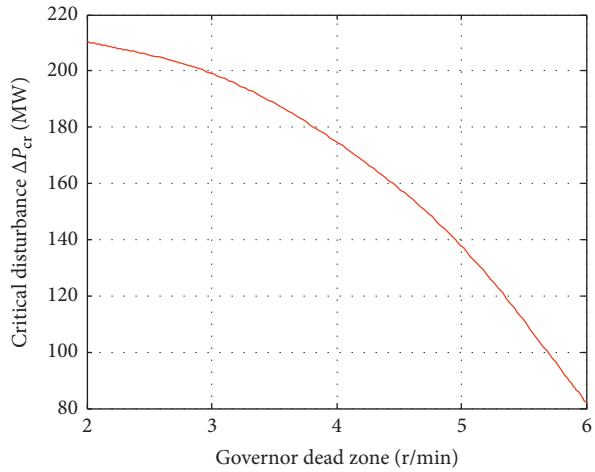

Figure 10: Critical disturbance amount curve after optimization of governor dead zone.

ΔP_{cr} = 304.5 MW, while the critical disturbance amount based on the nodal frequency characteristic surface before optimization is $\Delta P'_{cr}$ = 288.8 MW, which indicates that the frequency stability is significantly improved.

6. Conclusions

With the increasing proportion of photovoltaic power generation capacity in the total installed capacity of power systems, photovoltaic output is featured by randomness, intermittentness, no mechanical inertia, and "electric power electronics", which makes the control of power grids more complex and also profoundly changes the transient frequency stability characteristics of the system. In this paper, the influence mechanism of photovoltaic grid-connected power system frequency was analyzed, and the analysis method of frequency transient stability of photovoltaic grid-connected power system was proposed. The main conclusions are as follows:

(1) Based on the establishment of a BPA transient model of a photovoltaic grid-connected system, this paper explores the high- and low-frequency effects of the transient frequency of the system under the high permeability of photovoltaic under large disturbance. The mechanism analysis shows that as the photovoltaic permeability of the system increases, the problem of transient frequency stability in the system is easier to detect.

(2) A method for evaluating and analyzing the frequency characteristics of photovoltaic access nodes based on surface fitting is proposed. The IEEE 39-node standard system is used as an example to verify the effectiveness and correctness of the proposed method. Through the above method, the critical photovoltaic penetration rate of a certain node of the power grid can be determined, and the frequency dynamic characteristics of photovoltaic grid-connected nodes can be predicted and evaluated, which has great application reference value for determining the photovoltaic grid-connected points and its installed capacity in engineering practice. According to the simulation experiments and the accuracy check of the prediction results, it is verified that the prediction results have high accuracy.

(3) The measures for improving transient frequency stability based on optimization of frequency modulation parameters of large-capacity units are also proposed. The simulation results of IEEE 39-node standard system show that, by optimizing the adjustment coefficient of the large-capacity unit, the critical disturbance based on the nodal frequency characteristic surface can be increased, thereby significantly improving the frequency stability after photovoltaic grid connection.

Data Availability

No data were used to support this study.

Conflicts of Interest

The authors declare that there are no conflicts of interest regarding the publication of this paper.

Acknowledgments

This work was supported by the Technology Project of Yunnan Power Grid Co., Ltd. (0560002018030301XT00120).

References

[1] J. Lai, X. Lu, X. Yu, and A. Monti, "Stochastic distributed secondary control for ac microgrids via event-triggered communication," *IEEE Transactions on Smart Grid*, vol. 11, no. 4, pp. 2746–2759, 2020.

[2] J. Lai and X. Lu, "Nonlinear mean-square power sharing control for AC microgrids under distributed event detection," *IEEE Transactions on Industrial Informatics*, p. 1, 2020.

[3] J. Lai, X. Lu, X. Yu, and A. Monti, "Cluster-oriented distributed cooperative control for multiple AC microgrids," *IEEE Transactions on Industrial Informatics*, vol. 15, no. 11, pp. 5906–5918, 2019.

[4] J. Lai, H. Zhou, W. Hu, X. Lu, and L. Zhong, "Synchronization of hybrid microgrids with communication latency," *Mathematical Problems in Engineering*, vol. 2015, pp. 1–10, Article ID 586260, 2015.

[5] D. W. Liu, S. Y. Chen, and M. Ma, "A review of photovoltaic power generation system models," *Power System Technology*, vol. 35, no. 8, pp. 47–52, 2011.

[6] L. H. Stember, W. R. Huss, and M. S. Bridgman, "A methodology for photovoltaic system reliability & economic analysis," *IEEE Transactions on Reliability*, vol. R-31, no. 3, pp. 296–303, 1982.

[7] M. Ding, W. S. Wang, X. L. Wang et al., "Summary of the influence of large scale photovoltaic power generation on power system," *Proceedings of Chinese Society for Electrical Engineering*, vol. 34, no. 1, pp. 1–14, 2014.

[8] W. Zhang, T. Y. Xiang, A. Li et al., "Photovoltaic grid-connected transient stability calculation model based on MATLAB-PSASP," *Electrical Power Automation Equation*, vol. 32, no. 6, pp. 80–85, 2012.

[9] H. H. Wang, Y. Tang, C. Jing, J. Hou et al., "Combined modeling and equivalence of wind and light storage combined power generation system," *Proceedings of Chinese Society for Electrical Engineering*, vol. 31, no. 34, pp. 1–11, 2011.

[10] Y. Guan, J. C. Vasquez, J. M. Guerrero, Y. Wang, and W. Feng, "Frequency stability of hierarchically controlled hybrid photovoltaic-battery-hydropower microgrids," *IEEE Transactions on Industry Applications*, vol. 51, no. 6, pp. 4729–4742, 2015.

[11] F. Chan and H. Calleja, "Design strategy to optimize the reliability of grid-connected PV systems," *IEEE Transactions on Industrial Electronics*, vol. 56, no. 11, pp. 4465–4472, 2009.

[12] M. Liserre, R. Teodorescu, and F. Blaabjerg, "Stability of photovoltaic and wind turbine grid-connected inverters for a large set of grid impedance values," *IEEE Transactions on Power Electronics*, vol. 21, no. 1, pp. 263–272, 2006.

[13] H. Suyono and M. Zainuddin, "Injection impact of photovoltaic distributed generations (PVDG) on power distribution system stability," *Applied Mechanics and Materials*, vol. 785, pp. 403–408, 2015.

[14] J. Bank, B. Mather, J. Keller, and M. Coddington, "High penetration photovoltaic case study report," Office of Scientific & Technical Information, Technical Report, National Renewable Energy Laboratory (NREL), Denver, CO, USA, 2013.

[15] M. S. Widyan, "Operational performance stability of grid-connected photovoltaic generator via DC–DC converter and 48-pulse voltage source inverter," *International Journal of Modelling and Simulation*, vol. 37, no. 2, pp. 96–107, 2016.

[16] N. Kakimoto, S. Takayama, H. Satoh, and K. Nakamura, "Power modulation of photovoltaic generator for frequency control of power system," *IEEE Transactions on Energy Conversion*, vol. 24, no. 4, pp. 943–949, 2009.

[17] H. F. Zhou, L. Q. Ni, and T. S. Xu, "Study on dynamic characteristics of power system power frequency," *Power System Technology*, vol. 33, no. 16, pp. 58–62, 2009.

[18] Y. W. Du, "Research on frequency safety and stability characteristics and control of power grid under new energy access conditions," M. S. thesis, North China Electric Power University, Beijing, China, 2017.

[19] W. Q. Chen, X. N. Xin, and Z. P. Cheng, "Control technology of optical storage grid-connected power generation based on virtual synchronous generator," *Transactions of Nonferrous Metals Society of China*, vol. 33, no. 2, pp. 538–545, 2018.

[20] C. Zheng, S. Y. Wang, B. Q Zhang et al., "Dynamic frequency characteristics and countermeasures of photovoltaic high-permeability grid," *Power System Technology*, vol. 43, no. 11, pp. 4064–4073, 2019.

[21] C. G. Li, "Research on transient frequency stability assessment and control of power system," Ph. D. thesis, Shandong University, Jinan, China, 2012.